Viability assessment of a rigid wing airborne wind energy pumping system

6 authors, including:

Giovanni Licitra
University of Freiburg
12 PUBLICATIONS   **18** CITATIONS

SEE PROFILE

Jonas Koenemann
University of Freiburg
8 PUBLICATIONS   **163** CITATIONS

SEE PROFILE

Richard Ruiterkamp
Ampyx Power
54 PUBLICATIONS   **711** CITATIONS

SEE PROFILE

Moritz Diehl
University of Freiburg
94 PUBLICATIONS   **1,687** CITATIONS

SEE PROFILE

Some of the authors of this publication are also working on these related projects:

Project   Eco4Wind View project

Project   AWESCO - Airborne Wind Energy System Modelling, Control and Optimisation View project

Viability Assessment of a Rigid Wing Airborne Wind Energy Pumping System

Giovanni Licitra *, Jonas Koenemann *, Greg Horn †, Paul Williams *, Richard Ruiterkamp *, and Moritz Diehl ‡

* Ampyx Power B.V, The Hague, The Netherlands 2521AL

† Kitty Hawk, Mountain View, California

‡ Dept. of Microsystems Engineering and Dept. of Mathematics, University of Freiburg, Germany 79110

Email: g.licitra@ampyxpower.com, j.koenemann@ampyxpower.com, gregmainland@gmail.com, p.williams@ampyxpower.com, r.ruiterkamp@ampyxpower.com , moritz.diehl@imtek.uni-freiburg.de

Abstract—**Airborne wind energy is an emerging technology that is capable of harvesting wind energy by flying crosswind flight patterns with a tethered aircraft. Several companies are trying to scale-up their concept in order to be competitive in the energy market. However, the scaling process requires numerous iterations and trade-offs among the different components in terms of requirements that have to satisfy both technological and economical viability. In this paper, we show how to deal with this task by means of an optimal control approach combined with statistical analysis based on the established methods for conventional Wind Energy Conversion Systems. This approach is applied to a rigid wing pumping mode AWE System built by Ampyx Power B.V..**

I. INTRODUCTION

Airborne wind energy (AWE) is a novel technology emerging in the field of renewable energy systems. Using tethered aircraft for wind power generation, initially motivated by Loyd [1], represents a new concept for producing green energy via systems with high power-to-mass ratio, high capacity factors and with significant low installation costs with respect to the current established renewable technologies [2], [3]. Among the various possibilities for harvesting wind energy with a tethered wing [4], Ampyx Power B.V. [5] has been studying the promising approach of deploying a rigid wing in pumping cycles [6]. In a *pumping mode* AWE system (AWES), a *production phase* follows a *retraction phase* periodically. During the *production phase*, the aircraft exerts a high tension on the tether which is anchored to a ground station composed of a winch and an electric generator. The mechanical power is fed to the electric grid after electrical conversion. Due to finite tether length, a *retraction phase* is required where the tether is wound up by changing the flight pattern. In this phase less lifting force is generated so that significantly less energy needs to be invested in comparison to what has been gained during the *production phase*. An artist's rendering of the two main phases of a *pumping mode* AWES is shown in Fig. 1. In general, AWES need to be scaled-up in order to be attractive for investments as well as to be competitive with respect to conventional wind turbines. Such process is not trivial and it requires numerous assessments in terms of system feasibility, certification and economic viability due to the numerous variables that need to be taken into account simultaneously. In this
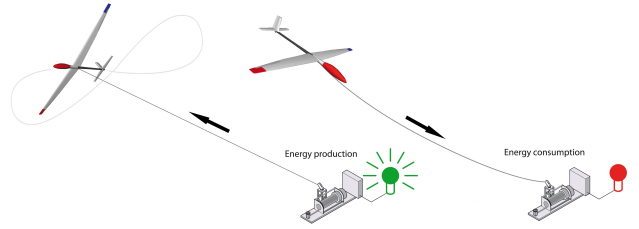

Fig. 1. Example of a pumping cycle with a *production* and *retraction phase*

paper, we propose an approach based on optimality principles that addresses systematically the viability assessment of a rigid wing pumping mode AWES for scaling-up purposes. The assessments rely on the proven concepts designed by Ampyx Power B.V. where the physical characteristics of the system can be found in [7]. In Section II, the mathematical model of the rigid wing pumping mode AWES is presented. In Section III the performance assessment is formulated as an Optimal Control Problem (OCP). In Section IV, a statistical analysis is computed by means of *power curve*, *Annual Energy Production* and *capacity factor*.

II. MATHEMATICAL MODEL

1) Wind Shear Modeling: For conventional and AWE systems, it is usually assumed that the wind speed w increases with height h above the ground. One common model of the wind speed is expressed via a logarithmic function equal to

$$w(h) = w_{h_{\text{ref}}} \frac{\ln(\frac{h}{h_r})}{\ln(\frac{h_{\text{ref}}}{h_r})} \,, h > h_{\text{ref}} \tag{1}$$

where h_{ref} is the height above the ground where the wind meter, which provides the wind speed measurement $w_{h_{ref}}$, is located. The surface roughness is denoted as h_r which accounts for the effects of obstacles protruding from the earth's surface. In this paper we assume that the AWE system is installed on an open field with some windbreaks more than 1 km away i.e. $h_r = 0.1$ [m] and $h_{\text{ref}} = 10$ [m] (more details in [8]).

A. Airborne Component Modeling

Let us consider a right-handed Cartesian coordinate system, where the vector $\vec{p} = [p_x, p_y, p_z]^\top$ represents the aircraft position w.r.t. the ground station located at the origin. The airborne component and the ground station are linked together via a tether of length l, hence both components are constrained to move along a manifold described as

$$c(t): \frac{1}{2}(\vec{p}^\top \vec{p} - l^2) = 0 \tag{2}$$

According to [9], one can model a rigid wing *pumping mode* AWES via a set of differential **F** and algebraic **G** equations by

$$\frac{d}{dt}\mathbf{x} = \mathbf{F}(\mathbf{x}, \mathbf{z}, \mathbf{u})$$
$$0 = \mathbf{G}(\mathbf{x}, \mathbf{z}, \mathbf{u}) \tag{3}$$

where $\mathbf{x} \in R^{n_x}, \mathbf{z} \in R^{n_z}$ are respectively differential and algebraic states and $\mathbf{u} \in R^{n_u}$ the control inputs. Since (2) represents a so called *holonomic constraint* i.e., a purely position-dependent constraint, one has to differentiate it twice in order to avoid rank deficiency in (3) i.e.

$$\dot{c}(t): \vec{v}^\top \vec{p} - l\dot{l} = 0 \tag{4a}$$
$$\ddot{c}(t): \dot{\vec{v}}^\top \vec{p} + \vec{v}^\top \vec{v} - \dot{l}^2 - l\ddot{l} = 0 \tag{4b}$$

where $\vec{v}$ is the translational velocity of the aircraft. Successively, a DAE index-1 formulation can be achieved after an index reduction procedure so that classical integration methods work efficiently [10]. The aircraft model expressed in the semi-explicit formulation is stated as follows:

$$\frac{d}{dt}\mathbf{x} = \begin{bmatrix} \vec{v} \\ m^{-1}\left[\vec{F}_a(\vec{v}, \vec{\omega_b}, R, l, \vec{\delta}) + \vec{F}_g + \vec{F}_t\right] \\ R \cdot \Omega \\ J^{-1}\left[\vec{M}_a(\vec{v}, \vec{\omega_b}, R, l, \vec{\delta}) - (\vec{\omega_b} \times J \cdot \vec{\omega_b})\right] \\ \vec{l}_t \\ \dot{\vec{\delta}} \end{bmatrix} \tag{5a}$$

$$0 = \dot{\vec{v}}^\top \vec{p} + \vec{v}^\top \vec{v} - \dot{l}^2 - l\ddot{l} \tag{5b}$$

Equation (5a) embeds the translational and rotational acceleration of the aircraft with mass m and inertia J, derived from Newton's second law. The gravity and tether forces are defined as $\vec{F}_g = [0, 0, mg]^\top$ and $\vec{F}_t = \lambda\vec{p}$ where λ denotes the tether tension while $\vec{F}_a$ and $\vec{M}_a$ stand for aerodynamic forces and moments. $R \cdot \Omega$ represents the time evolution of the Direct Cosine Matrix (DCM) used to describe the orientation of the aircraft where R is the transformation matrix from the inertial frame to the body frame and Ω is the skew symmetric matrix of the rotational velocity $\omega_b = [p, q, r]^\top$. $R = [\hat{e}_x, \hat{e}_y, \hat{e}_z]$ is composed of the unit vectors $\hat{e}_{x,y,z}$ that point along the longitudinal, transversal, and vertical axes of the wing. The vector $\vec{l}_t = [\dot{l}, \ddot{l}, \dddot{l}]^\top$ gathers the tether components which are the tether speed $\dot{l}$, acceleration $\ddot{l}$ and jerk $\dddot{l}$. In the same way, the vector $\vec{\delta}$ collects the rates of control surface deflection of aileron δ_a, elevator δ_e, and rudder δ_r. Finally, the set
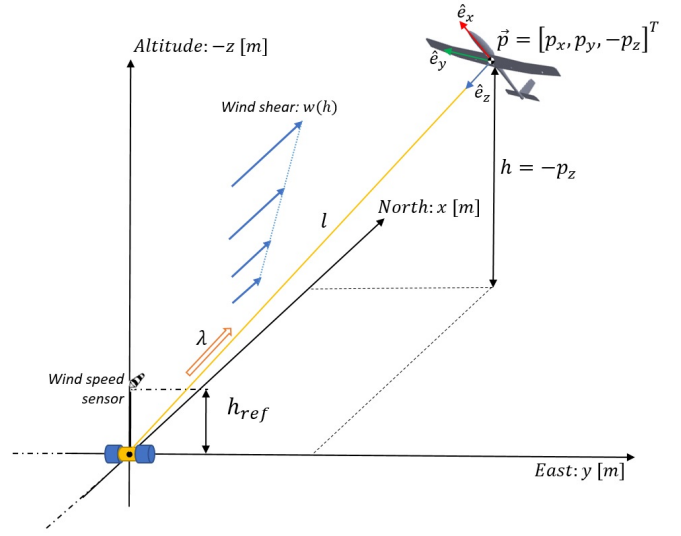

Fig. 2. Coordinate system and vector conventions for the rigid-wing AWES in pumping mode. For the earth fixed coordinate frame and the aircraft's body frame the north-east-down convention is used.

of algebraic equations $\mathbf{G}(.)$ is given simply by (4b). Fig. 2 shows the sketch of a setting in which the rigid wing AWES operates indicating the most important coordinates. Finally, differential/algebraic states and control inputs are summarized as

$$\mathbf{x} = \left[\vec{p}, \vec{v}, R, \vec{\omega_b}, l, \dot{l}, \ddot{l}, \delta_a, \delta_e, \delta_r\right]^\top \in \Re^{24}$$
$$\mathbf{z} = \lambda \in \Re^1 \tag{6}$$
$$\mathbf{u} = \left[\dot{\delta_a}, \dot{\delta_e}, \dot{\delta_r}, \dddot{l}\right]^\top \in \Re^4$$

B. Aerodynamic Forces and Moments

In this section, we describe a mathematical model related to the aerodynamic forces $\vec{F}_a$ and moments $\vec{M}_a$. Assuming that the wind direction is pointing in north direction as shown in Fig. 2 i.e. $\vec{v}_w = [w(h), 0, 0]^\top$, let us define the relative velocity of the aircraft w.r.t. the wind expressed in the inertial frame

$$\vec{v}_r = \vec{v} - \vec{v}_w \tag{7}$$

then the relative velocity expressed in body frame is given by

$$\vec{v}_b = R \cdot \vec{v}_r = [u, v, w]^T \tag{8}$$

By means of (8), it is possible to define the true airspeed V_a, angle of attack α and angle of side-slip β as follows

$$V_a = \|\vec{v}_b\| \;, \; \alpha = \arctan\left(\frac{w}{u}\right) \;, \; \beta = \arcsin\left(\frac{v}{V_a}\right) \tag{9}$$

Then, the aerodynamic properties can be expressed in a compact notation by

$$\vec{F}_a = \frac{\rho S V_a^2}{2}\left(C_L\hat{v}_{C_L} - C_D\,\hat{v}_{C_D} - C_Y\hat{v}_{C_Y}\right) \tag{10a}$$

$$\vec{M}_a = \frac{\rho S V_a^2}{2}\left[C_l, C_m, C_n\right]^T \tag{10b}$$

where ρ is the air density, S the wing area, C_L, C_D, C_Y the *force coefficients* of lift, drag and side forces where their directions are given by the unit vectors $\hat{v}_{C_L}, \hat{v}_{C_D}, \hat{v}_{C_Y}$ defined below

$$\hat{v}_{C_L} = (\hat{e}_y \times \hat{v}_r), \ \hat{v}_{C_D} = \hat{v}_r, \ \hat{v}_{C_Y} = (\hat{e}_y \times \hat{v}_r) \times \hat{v}_r \quad (11)$$

with $\hat{v}_r = \vec{v}_r / ||\vec{v}_r||$. The *moment coefficients* C_l, C_m, C_n are related to the roll, pitch and yaw motion; in the aerospace field, force and moment coefficients are called *aerodynamic coefficients* and they are usually expressed as a combination of $\vec{\omega}_b, \vec{\delta}, \alpha, \beta$. As far as it regards our model, the aerodynamic coefficients are defined as follows

$$C_L = \Sigma_{i=0}^{3} C_{L_i} \alpha^i \tag{12a}$$
$$C_D = \Sigma_{i=0}^{4} C_{D_i} \alpha^i + C_{D_t} \tag{12b}$$
$$C_Y = C_{Y_\beta} \beta \tag{12c}$$
$$C_l = C_{l_\beta} \beta + C_{l_{\delta_a}} \delta_a + C_{l_{\delta_r}} \delta_r + C_{l_p} \hat{p} + C_{l_r} \hat{r} \tag{12d}$$
$$C_m = C_{m_\alpha} \alpha + C_{m_{\delta_e}} \delta_e + C_{m_q} \hat{q} + C_{m_0} \tag{12e}$$
$$C_n = C_{n_\beta} \beta + C_{n_{\delta_a}} \delta_a + C_{n_{\delta_r}} \delta_r + C_{n_p} \hat{p} + C_{n_r} \hat{r} \tag{12f}$$

where $\hat{p}, \hat{q}, \hat{r}$ are the normalized body rates and they are equal to

$$\hat{p} = \frac{b \, p}{2 V_a} \ , \ \hat{q} = \frac{\bar{c} \, q}{2 V_a} \ , \ \hat{r} = \frac{b \, r}{2 V_a} \tag{13}$$

with b the wing span and $\bar{c}$ the aerodynamic chord. Finally, the coefficients C_{**} in (12) are known as *aerodynamic derivatives* which are retrieved from Computational fluid dynamics (CFD) [11] or lifting line methods [12] and verified by an extensive flight test campaign [13]. Usually, aerodynamic coefficients are stored as look-up tables. In order to ensure smoothness of the parameters in an OCP framework, we compute the polynomial coefficients for C_L and C_D in (12a-12b) by data fitting of the look-up tables in the region of the flight envelope as shown in Fig. 3. Finally, one has to point out that in (12b) the coefficient C_{D_t} represents the normalized tether drag contribution, determined analytically via a finite element approach as shown in the next section.

C. Tether Drag Modeling

One of the main differences between a conventional and a tethered aircraft is the presence of the tether which induces additional drag, moments (if the tether is not placed in the center of gravity of the aircraft) and weight. As a consequence, tether drag modeling is crucial for computing accurate performance assessments. For this purpose, let us consider the *reel-out phase* i.e. when the aircraft pulls the tether; in general the side-slip angle β causes additional drag, hence for an optimal flight one aims to keep $\beta \approx 0$. When β is small, the drag acts mainly in the longitudinal plane of the aircraft which means that we can use a 2D representation as in Fig. 4. Furthermore, let us assume that the cable airspeed velocity V_t is a linear function of both l and aircraft velocity V_a , and its direction is always orthogonal to the cable, i.e.

$$V_t \approx \frac{s}{l} V_a \cos(\gamma + \psi) \quad s \in [0, l] \tag{14}$$

where s is a spatial coordinate along the cable of length l, γ the flight path angle, $\psi = \arccos(\frac{h}{l})$ the zenith angle, Φ the elevation angle. The drag force for an elemental portion $\mathrm{d}s$ of the cable is

$$D_s = \frac{1}{2} \rho V_t^2 C_{D_N} d \, \mathrm{d}s \tag{15}$$

where $C_{D_N} = 1.2$ is the drag coefficient and d is the tether diameter. The moment provided by the tether drag around the ground station is

$$M_{D_s} = D_s \, s = \left(\frac{1}{2} \rho V_t^2 C_{D_N} d \, \mathrm{d}s \right) s \tag{16}$$

Thus, the total moment due to drag is given by the integral along the tether which is

$$\begin{aligned} M_{D_t} &= \int_0^l \left(\frac{1}{2} \rho \left(\frac{s}{l} V_a \cos(\gamma + \psi) \right)^2 C_{D_N} d \, s \right) \mathrm{d}s = \\ &= \frac{1}{8} \rho V_a^2 \cos^2(\gamma + \psi) C_{D_N} d \, l^2 \end{aligned} \tag{17}$$

with corresponding drag force on the aircraft

$$D_t = \frac{1}{8} \rho V_a^2 \cos^2(\gamma + \psi) C_{D_N} d \, l \tag{18}$$

In the aerospace field, the convention is to normalize forces by dividing by dynamic pressure times the wing surface area, i.e. $\frac{1}{2} \rho V_a^2 S$. Hence, the tether drag coefficient normalized w.r.t. the aircraft in (12b) is

$$C_{D_t} = \frac{C_{D_N} d}{4S} \cos^2(\gamma + \psi) \, l \tag{19}$$

Finally, note that (19) represents the tether drag approximation used in [7], [14] with additional informations regarding the zenith and flight path angle.
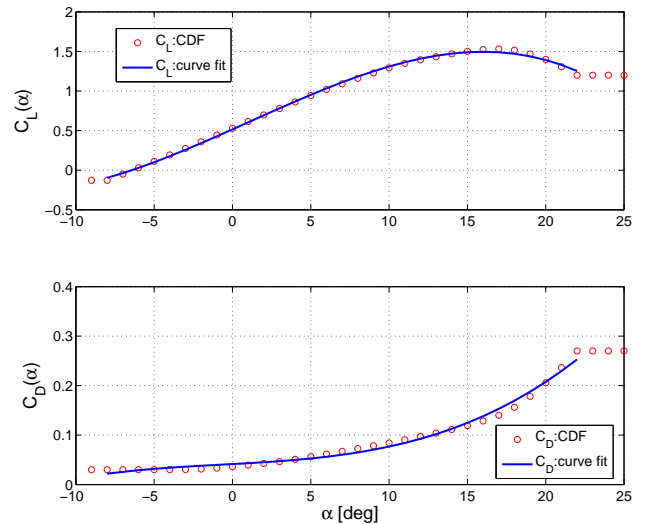

Fig. 3. Polynomial interpolation of C_L and C_D within the flight envelope
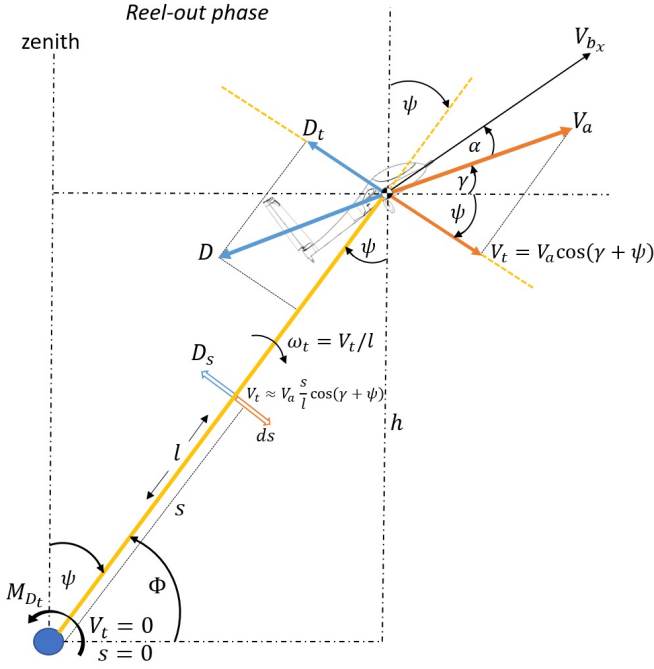
Fig. 4. Schematic model that is being used for calculating the tether drag. The total drag D_t results from integrating the drag components D_s along the tether coordinate s.

D. Ground Station Modeling

The ground station is basically composed of a winch mechanism connected to an electric motor (see Fig. 5). The mechanical power generated by the tether tension λ is equal to

$$P_m = \tau_d \cdot \omega_d \qquad (20)$$

where $\tau_d = \lambda \cdot r_d$, $\omega_d = \dot{l} \cdot r_d$ are the torque and the angular velocity around the winch with r_d the drum radius, while the electrical power P_e can be coupled to P_m by means of the motor efficiency η as follows

$$P_e = \eta\left(\tau_d, \omega_d\right) \cdot P_m, \quad 0 < \eta(.) < 1 \qquad (21)$$

In general, the motor efficiency $\eta(.)$ is mainly a function of τ_d, ω_d as well as the operation mode (*reel-in* phase $\Leftrightarrow$ *motor* mode | *reel-out* phase $\Leftrightarrow$ *generator* mode). Efficiency characteristics can be retrieved both from data-sheets and via extensive tests bench. According to [15], P_e can be expressed with reasonable degree of accuracy as a linear combination of τ_d and ω_d as

$$P_e = p_0 + p_{\omega_2}\,\omega_{\text{drum}}^2 + p_{\tau_2}\,\tau_{\text{drum}}^2 + p_{\tau\omega}\,\omega_{\text{drum}}\tau_{\text{drum}} \qquad (22)$$

where the coefficients $p_0, p_{\omega_2}, p_{\tau_2}, p_{\tau\omega}$ are determined by data fitting. However, in this paper we assume a constant efficiency $\eta = 94\%$ coming from a data-sheet, since test bench measurements were not available. One has to make two remarks:

- we are implicitly neglecting the ground station dynamics, in other words the transient responses are assumed much faster then the dynamics of the airborne component.

- the data-sheet does not provide information regarding the efficiency in the case of low ω_d and high τ_d where an efficiency significantly lower than the assumed values in this work is expected.

III. FORMULATION OF AN OPTIMAL CONTROL PROBLEM FOR PERFORMANCE ASSESSMENT

In general, design of AWES aims at maximizing the average power output along the trajectory, which usually has either a circular or a lemniscate shape. Here we propose a formulation of an OCP for maximizing the power output of a rigid wing AWES in pumping mode

$$\underset{\mathbf{x}(.),\mathbf{z}(.),\mathbf{u}(.),T}{\text{minimize}} \quad \frac{1}{T}\int_0^T \left(-P_e(t) + \|\mathbf{u}(t)\|_{\Sigma_{\mathbf{u}}^{-1}}^2 + \sigma_\beta^{-1}\beta(t)^2\right)dt \qquad (23a)$$

$$\begin{aligned}
\text{subject to} \quad & \dot{\mathbf{x}}(t) = \mathbf{F}(\mathbf{x}(t), \mathbf{z}(t), \mathbf{u}(t)), & t \in [0,T] \quad (23b) \\
& 0 = \mathbf{G}(\mathbf{x}(t), \mathbf{z}(t), \mathbf{u}(t)), & t \in [0,T] \quad (23c) \\
& \vec{\Delta}_m \leqslant \vec{\Delta}(t) \leqslant \vec{\Delta}_M, & t \in [0,T] \quad (23d) \\
& \vec{A}_m \leqslant \vec{A}(t) \leqslant \vec{A}_M, & t \in [0,T] \quad (23e) \\
& \vec{V}_m \leqslant \vec{V}(t) \leqslant \vec{V}_M, & t \in [0,T] \quad (23f) \\
& \vec{G}_m \leqslant \vec{G}(t) \leqslant \vec{G}_M, & t \in [0,T] \quad (23g) \\
& \lambda_m \leqslant \lambda(t) \leqslant \lambda_M, & t \in [0,T] \quad (23h) \\
& h_m \leqslant h(t) \leqslant h_M, & t \in [0,T] \quad (23i) \\
& T_m \leqslant T \leqslant T_M, & t \in [0,T] \quad (23j) \\
& c(t) = \dot{c}(t) = \Xi_0(t) = 0, & t = 0 \quad (23k) \\
& \mathbf{r}\left(\mathbf{x}(0), \mathbf{x}(T)\right) = 0 & (23l)
\end{aligned}$$

The cost function (23a) takes into account electrical power P_e along the pattern of time length T; control inputs $\mathbf{u}$ are penalized via the regulation term $\Sigma_{\mathbf{u}}^{-1}$ in order discourage aggressive maneuvers while the square of the side-slip beta β is penalized by σ_β^{-1} in order to avoid additional drag and allow the assumption of decoupled lateral and longitudinal dynamics for feedback control purposes [16]. The constraints are mainly related to the physical limitations of the overall system. Moreover periodicity and consistency conditions have
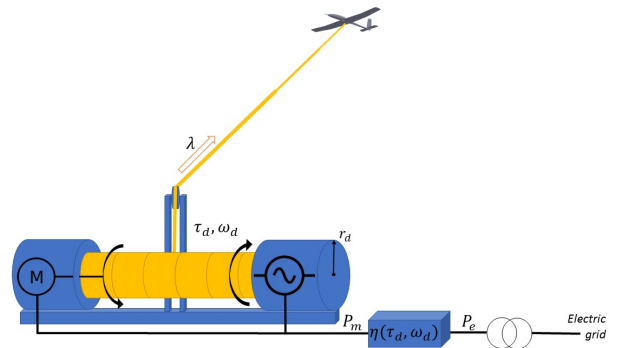

Fig. 5. The ground station converts the mechanical energy from tether tension into electrical power and feeds it to the grid.

to be properly imposed in order to obtain a well-posed OCP. The constraints in (23) are briefly described below:

- The OCP is subject to the model dynamics defined in section II-A in (23b-23c);
- Deflection as well as rate control surfaces $\vec{\Delta} = [\vec{\delta}, \dot{\vec{\delta}}]$ are subject to limitations both in angles and speeds, related to the installed servo motors (23d);
- The aerodynamic states $\vec{A} = [V_a, \alpha, \beta]$ need to be bounded within the flight envelope in order to avoid stall phenomena as well as undesirable lateral forces caused mainly by the fuselage (23e) [16];
- The bounds of translational and angular velocity $\vec{V} = [\vec{v}, \vec{\omega}_b]$ are defined in function of structural analysis related to the airborne component (23f);
- The vector $\vec{G} = [l, \dot{l}, \ddot{l}, \tau, \omega_w]$ collects all the constraints related to the intrinsic characteristics of the ground station (23g);
- Tether tension λ need to be bounded for model consistency, to avoid sag effects, to reduce mechanical stress on the airborne component, and to mitigate risk of tether damage (23h);
- The altitude h has a lower bound for both safety and certification requirements (23i);
- The pattern time T is chosen by the OCP and bounded according to practical experience (23j);
- Consistency conditions related to the algebraic equation shown in (2) need to be enforced, while $\Xi_0 = R^\top R - I$ preserves the orthonormality of R; however only the main diagonal and the three lower components of Ξ_0 are enforced in order to avoid LICQ deficiency (23k).
- The periodicity condition is formally enforced by $\tilde{\mathbf{x}}_0 - \tilde{\mathbf{x}}_F = 0$, however, because of the non-minimal coordinates, this condition would produce an over-constrained problem. Thus, the periodicity condition is in our case

$$\mathbf{r}\left(\mathbf{x}(0), \mathbf{x}(T)\right) = \begin{bmatrix} p_{y_0} - p_{y_T} \\ p_{z_0} - p_{z_T} \\ v_{y_0} - v_{y_T} \\ v_{z_0} - v_{z_T} \\ \vec{\omega}_{b_0} - \vec{\omega}_{b_T} \\ l_0 - l_T \\ \dot{l}_0 - \dot{l}_T \\ \ddot{l}_0 - \ddot{l}_T \\ \vec{\delta}_0 - \vec{\delta}_T \\ R_0^\top R_T - I \end{bmatrix} \quad (24)$$

where in $R_0^\top R_T - I$ only the three upper off-diagonal components are constrained. As in (23k), the subscripts 0 and T refer to the initial and final time.

Since the OCP (23) is non-convex due to the nonlinear dynamic constraints, the Non Linear Program (NLP) solver must be initialized with an educated initial guess. Such an initial guess can be computed via an *homotopy process*, as shown in [17] and in [18] for the specific case. The solution to the OCP (23) provides several insights regarding the plant, e.g. the existence of a feasible trajectory given by a set of physical
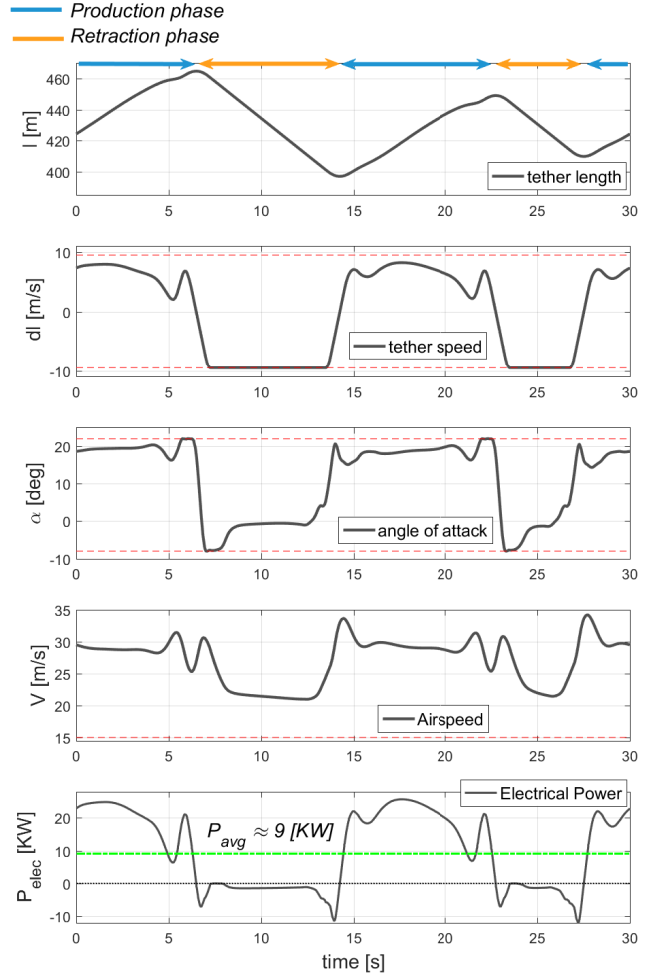

Fig. 6. Typical optimized pattern for the 2nd generation of Prototype designed by Ampyx Power B.V. During the *production phase* (blue arrows), the aircraft flies with a high airspeed and high angle of attack; such combination provides a lift force which is used for drive the generator located in the ground by pulling the tether. The *retraction phase* (orange arrows) is performed with the maximum reel-in speed available in order to minimize the reel-in time. During the *retraction phase*, the angle of attack is low so that the lift force is minimized. Along this pattern, the average power P_{AVG} is roughly 9KW (green line).

parameters and constraints as well as his optimal behavior (Fig. 6), in other words it provides performance assessments for a certain system configuration. Fig. 7 shows a typical power optimal trajectory overlapped with the test centre located in Kraggenburg (NL) used by Ampyx Power B.V.. The OCP was implemented via the *Flight Optimization Toolbox* designed for AWES and freely available in [19]. The toolbox is based on *CasADi* [20] and *IPOPT* as NLP solver [21], implemented in a Matlab Environment. The toolbox supports Direct Collocation Techniques with *RADAU* collocation points. A toolbox with similar features and based on *CasADi* but in Python is the *RAWESOME Airborne Wind Energy Simulation, Optimization and Modeling Environment* [22].
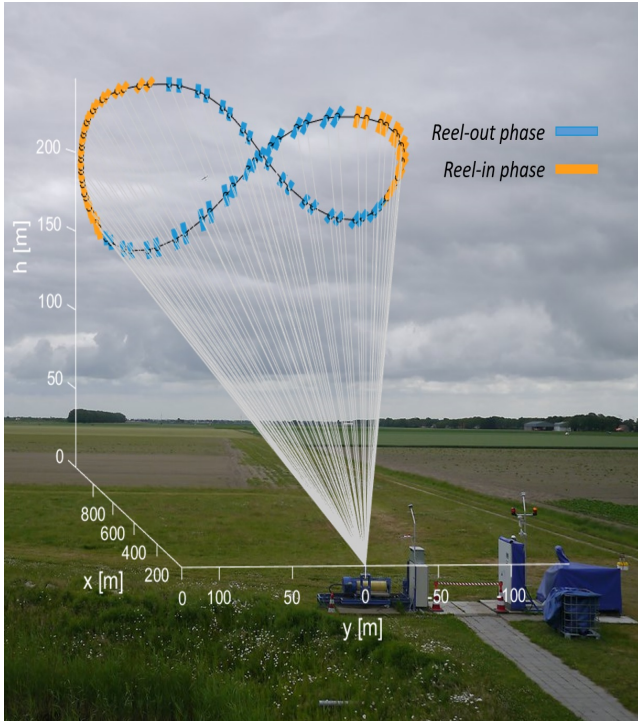
Fig. 7. Typical optimized-power trajectory related to the 2nd generation of Prototype designed by Ampyx Power B.V.

IV. STATISTICAL ANALYSIS

In order to assess the viability of a given rigid wing pumping mode AWES, one can perform an analysis via a statistical approach employed for wind turbines. It is usual for Wind Energy Conversion Systems to define the *power curve* i.e. the net power produced along a range of wind speeds of interest. The power curve can be determined using (23) where the measured wind speed $w_{h_{ref}}$, shown in (1), is used as a parameter. In our case, the net electrical power output refers to the average power that the system can generate over the whole pumping cycle, under optimal conditions. Once the *power curve* is known, one can compute the performance of the system at a given location in terms of Annual Energy Production (E_{AEP}) by means of wind distributions. Usually, wind distributions are approximated by Weibull or Rayleigh distributions, where the parameters can be tuned based on either previous measurements related to a specific location or using the international standard IEC 61400-1. In this paper we take into account the wind distribution wind class-1A and 2A [23]. The results of the statistical analysis are shown in Fig. 8. Finally, if one assumes that the energy has a time-independent tariff, it is possible to describe the performance of a system by the so called *capacity factor* c_f equal to

$$c_f = \frac{E_{AEP}}{8760\,h \cdot P_{\max}} \qquad (25)$$

which is defined as the number of hours h per year (8760 for a non-leap year) multiplied by the maximum power output, in our case $P_{\max} \approx 11$ [KW].
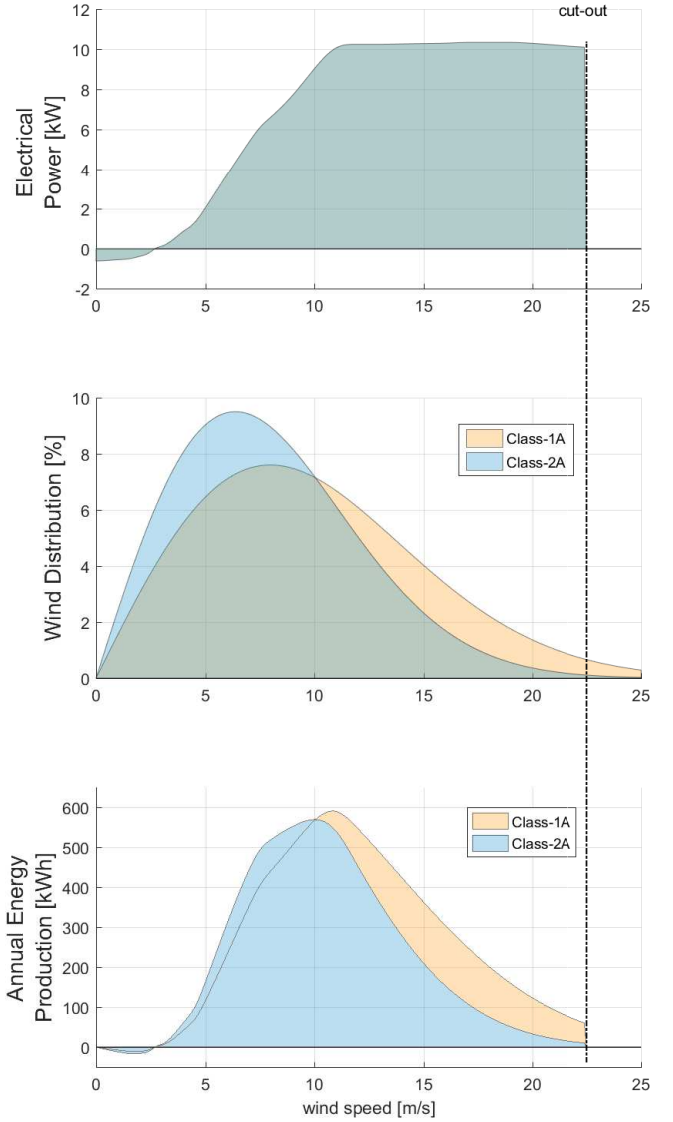

Fig. 8. From the top: power curve related to the Pumping mode AWES; Weibull probability density function for both wind class 1A and 2A; Annual Energy Production (AEP)

The results in Table I show that small rigid wing pumping model AWES can provide energy for approximatively 15 households under the assumption that the global average electricity consumption for households is roughly 3.500 kWh/year [25]. Note that the plant that was taken into account is used as case-study for testing and verification purposes only. Once these informations are available for a given pumping mode AWES, one can perform further analysis related to Operating and Maintenance costs (O&M) as well as market factors and

TABLE I
STATISTICAL ANALYSIS RESULTS

wind class	1A	2A
c_f	64 %	53 %
E_{AEP}	58 MWh	49 MWh
Powered-Households	16	14

economic viability indicators (for more details the reader is referred to [24]).

V. CONCLUSION

In this paper, the annual energy production and the capacity factor of a rigid wing pumping mode AWE system have been determined. In order to perform this analysis, we described the mathematical model of the ground station, the tether and the airborne component. Assessing the performance of the plant involves numerous parameters that need to be taken into account simultaneously. For this reason, an optimal control approach has been chosen. We solved a sequences of optimal control problems for a range of wind speeds. The results have shown that a small scale AWE system with a wing area of $5.5\mathrm{m}^2$ can produce about 50 MWh per year which corresponds to the power of 15 households. With the proposed optimal control approach, many decisional tasks e.g. the scaling up of AWE systems can be facilitated.

ACKNOWLEDGMENT

REFERENCES

[1] M. L. Loyd, "Crosswind kite power (for large-scale wind power production)," *Journal of energy*, vol. 4, no. 3, pp. 106–111, 1980.
[2] M. Diehl, R. Schmehl, and U. Ahrens, *Airborne Wind Energy. Green Energy and Technology*. Springer Berlin Heidelberg, 2014.
[3] L. Fagiano and M. Milanese, "Airborne wind energy: an overview," in *American Control Conference (ACC), 2012*. IEEE, 2012, pp. 3132–3143.
[4] M. Diehl, "Airborne wind energy: Basic concepts and physical foundations," in *Airborne Wind Energy*. Springer, 2013, pp. 3–22.
[5] (2016) Ampyx power: Airborne wind energy. [Online]. Available: https://www.ampyxpower.com/
[6] P. Williams, B. Lansdorp, R. Ruiterkamp, and W. Ockels, *Modeling, simulation, and testing of surf kites for power generation*. American Institute of Aeronautics and Astronautics, 2008.
[7] G. Licitra, S. Sieberling, S. Engelen, P. Williams, R. Ruiterkamp, and M. Diehl, "Optimal control for minimizing power consumption during holding patterns for airborne wind energy pumping system." Proceedings of the European Control Conference, 2016.
[8] C. L. Archer, "An introduction to meteorology for airborne wind energy," in *Airborne wind energy*. Springer, 2013, pp. 81–94.
[9] S. Gros and M. Diehl, "Modeling of airborne wind energy systems in natural coordinates," in *Airborne wind energy*. Springer, 2013, pp. 181–203.
[10] U. M. Ascher and L. R. Petzold, *Computer methods for ordinary differential equations and differential-algebraic equations*. Siam, 1998, vol. 61.
[11] H. K. Versteeg and W. Malalasekera, *An introduction to computational fluid dynamics: the finite volume method*. Pearson Education, 2007.
[12] J. D. Anderson Jr, *Fundamentals of aerodynamics*. Tata McGraw-Hill Education, 2010.
[13] J. Mulder, J. Sridhar, and J. Breeman, "Identification of dynamic system-application to aircraft nonlinear analysis and manoeuvre design," Technical Report AG 300, AGARD, Tech. Rep., 1994.
[14] S. Sieberling and R. Ruiterkamp, "The powerplane an airborne wind energy system-conceptual operations," in *11th AIAA Aviation Technology, Integration, and Operations (ATIO) Conference, including the AIAA Balloon Systems Conference and 19th AIAA Lighter-Than*, 2011, p. 6909.
[15] J. Stuyts, G. Horn, W. Vandermeulen, J. Driesen, and M. Diehl, "Effect of the electrical energy conversion on optimal cycles for pumping airborne wind energy," *IEEE Transactions on Sustainable Energy*, vol. 6, no. 1, pp. 2–10, 2015.
[16] J. Mulder, W. Van Staveren, and J. van der Vaart, *Flight dynamics (lecture notes): ae3-302*. TU Delft, 2000.
[17] G. Horn, S. Gros, and M. Diehl, "Numerical trajectory optimization for airborne wind energy systems described by high fidelity aircraft models," in *Airborne wind energy*. Springer, 2013, pp. 205–218.
[18] S. Gros, M. Zanon, and M. Diehl, "A relaxation strategy for the optimization of airborne wind energy systems," in *Control Conference (ECC), 2013 European*. IEEE, 2013, pp. 1011–1016.
[19] J. Koenemann. (2017) Flight optimization toolbox. [Online]. Available: https://github.com/JonasKoenemann/optimal-control
[20] J. Andersson, "A General-Purpose Software Framework for Dynamic Optimization," PhD thesis, Arenberg Doctoral School, KU Leuven, Department of Electrical Engineering (ESAT/SCD) and Optimization in Engineering Center, Kasteelpark Arenberg 10, 3001-Heverlee, Belgium, October 2013.
[21] A. Wächter and L. T. Biegler, "On the implementation of an interior-point filter line-search algorithm for large-scale nonlinear programming," *Mathematical programming*, vol. 106, no. 1, pp. 25–57, 2006.
[22] G. Horn. (2017) the rawesome airborne wind energy simulation, optimization and modeling environment. [Online]. Available: https://github.com/ghorn/rawesome
[23] J. F. Manwell, J. G. McGowan, and A. L. Rogers, *Wind energy explained: theory, design and application*. John Wiley & Sons, 2010.
[24] J. Heilmann and C. Houle, "Economics of pumping kite generators," in *Airborne Wind Energy*. Springer, 2013, pp. 271–284.
[25] (2017) World energy council. [Online]. Available: https://www.worldenergy.org/